DYNAMIC MODELING AND SIMULATION OF A 14-DOF WHEELED AGRICULTURAL ROBOT
/
基于十四自由度轮式农业机器人动力学建模与仿真

Mengmeng NI, Fanjun MENG, Fa SUN, Zhisheng ZHAO, Lili YI*), Fanxia KONG*)
Shandong University of Technology, Collage of Agricultural Engineering and Food Science, Zibo, China

Corresponding author: Lili YI; Tel: +86 18553308656; E-mail: yili0001@sdut.edu.cn
DOI: https://doi.org/10.35633/inmateh-77-61

Keywords: *14-degree-of-freedom, Tire Model, Ackermann steering geometry, suspension system*

ABSTRACT

To address the requirements for automation and intelligence of agricultural robots, this paper develops a 14-degree-of-freedom dynamic model for wheeled agricultural robots. The model aims to provide a dynamic modeling foundation under the framework of modern control theory for the automation and intelligence of wheeled agricultural robots. It incorporates the Ackermann steering mechanism, MacPherson independent suspension system, tire model, and deformable soil model based on Bekker's formula. The vertical tire pressure is calculated using the deformable soil model via Bekker's formula, while tire forces are predicted by combining the tire slip angle and slip ratio with the Magic Formula Tire Model. By analyzing the force transmission effect of the suspension system, integrating the center-of-mass coupling effect analysis and the robot body model equations, the precise prediction of the attitude and motion trajectory of the wheeled agricultural robot is achieved. A co-simulation experiment using MATLAB and CarSim under the double lane change (DLC) condition is designed for validation. Experimental results demonstrate that the proposed model exhibits high consistency with the CarSim simulation results. The mean absolute errors (MAE) are 0.327° for steering wheel angle, 0.677°/s for yaw rate, 0.691° for body roll angle, and 0.944 m/s² for lateral acceleration. All errors are less than 1.5, meeting the requirements of dynamic simulation. This model can effectively predict the body attitude of wheeled agricultural robots and lay a foundation for the subsequent development of optimal control algorithms for agricultural robots.

摘要

针对农业机器人自动化与智能化的需求，本文构建了一套十四自由度轮式农业机器人动力学模型，旨在为轮式农业机器人的自动化与智能化提供现代控制学理论框架下的动力学模型基础。该模型涵盖了阿克曼转向机构、麦弗逊独立悬架系统、轮胎模型以及 Bekker 公式的可变形土壤模型等。通过 Bekker 公式的可变形土壤模型计算轮胎正压力，将轮胎侧边角和滑移率结合魔术公式轮胎模型（Magic Formula Tire Model）预测轮胎力，分析悬架系统对力的传递效应，结合重心耦合效应分析及机器人身体模型公式，实现了对轮式农业机器人姿态及运动轨迹的精准预测。设计双移线（DLC）工况下 MATLAB 与 CarSim 联合仿真实验进行验证，实验结果表明：该模型与 CarSim 仿真结果一致性较高，转向盘转角平均绝对误差（MAE）为 0.327°、横摆角速度为 0.677°/s、车身侧倾角为 0.691°、侧向加速度为 0.944 m/s²，所有误差均小于 1.5，满足动力学仿真需求。该模型可有效预测轮式农业机器人机身姿态，为后续农业机器人最优控制算法开发奠定基础。

INTRODUCTION

Under the dual pressures of the escalating global food security crisis and the structural shortage of agricultural labor, the automation of agricultural equipment has become a strategic technical approach to break the bottleneck of agricultural productivity growth *(Daum T., 2024)*. High-precision motion control of agricultural robots directly determines field operation quality, and establishing a high-fidelity dynamic model is a prerequisite for achieving precise control *(Kayacan et al., 2015)*.

In recent years, agricultural robots have been widely applied in field operations such as seeding, fertilization, weeding, and harvesting, with dynamic modeling being a core research focus. Existing studies on agricultural robot dynamics can be categorized into three directions: simplified low-DOF models, multi-body dynamics models, and soil-tire interaction models. For low-DOF models, *Long et al., (2022),* proposed a 2-DOF steering dynamic model for agricultural tractors, which realizes basic path tracking but ignores vertical vibration and tire-soil deformation, leading to significant errors in bumpy farmland.

Nigwal et al., (2023), developed a 7-DOF full-vehicle vibration model, which improves ride comfort prediction but lacks consideration of wheel rotation and lateral-longitudinal coupling effects. *(Hassaan et al. 2015)* established a 10-DOF multi-body coupling model, which enhances the description of body motion but still fails to reflect the dynamic characteristics of agricultural tires on deformable soil.

For soil-tire interaction models, *Roşca et al., (2022),* proposed a traction model considering tire-soil contact deformation, which accurately predicts traction force on soft soil but is difficult to integrate with full-vehicle dynamics due to its complexity. *Cha et al., (2024),* optimized the tire model for high-speed handling, but it is not applicable to low-speed agricultural operations on uneven terrain. In terms of application scenarios, most existing models are verified on hard roads (e.g., asphalt pavement) rather than actual farmland, resulting in poor adaptability to complex terrain such as weed-covered fields and gully-crossed plots *(Reimpell et al., 2001)*.

Although these studies have made progress in specific fields, there are still obvious limitations: (1) The degree of freedom setting is overly dependent on highway vehicle standards, ignoring the vertical bouncing of tires and the rotation of wheel axes under farmland conditions; (2) The tire model uses passenger car parameters instead of agricultural tires, failing to reflect the traction and damping characteristics on deformable soil; (3) The research on multi-field coupling (mechanical, soil, dynamic) is insufficient, leading to inaccurate attitude prediction in actual operations. To address these issues, this study constructs a 14-DOF dynamic model. By defining the vertical displacement degrees of freedom for the four sets of suspensions and integrating the Bekker formula model to characterize the bearing and deformation properties of farmland soil, a dynamic model tailored for farmland operation scenarios is constructed, which accurately simulates the influence of complex and deformable farmland surfaces on the vehicle body attitude.

MATERIALS AND METHODS

The model proposed in this paper is mainly divided into four parts: the steering mechanism model, the tire model, the suspension model, and the robot body model. The data relationships between these modules are shown in the following figure:

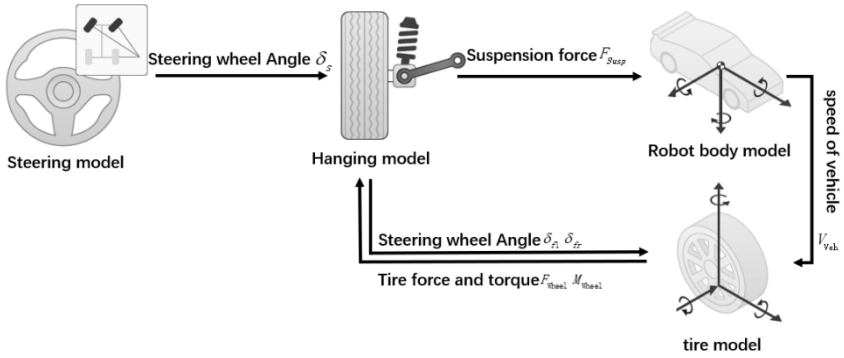

Fig. 1 - Inter-module data flows of a 14-DOF Wheeled Agricultural Robot

As shown in Fig. 1, the steering mechanism adopts an Ackermann steering configuration to control the wheel angles. The sideslip angle can be calculated from the steering-wheel angle δ_s by accounting for the effects of the steering mechanism and the MacPherson suspension system.

The tire model used in the figure adopts the Magic Formula Tire Model, which can predict the tire forces F_{wheel} and tire moments M_{wheel} based on the sideslip angle α and slip ratio κ. The slip ratio κ is calculated from the vehicle speed V_{eh} and wheel speed V_{wheel}. The sideslip angle α is calculated from the front-left wheel angle δ_{fl} and front-right wheel angle δ_{fl}.

The tire forces must be transmitted to the robot body through the suspension system, and this process involves the conversion between the tire forces F_{wheel}& tire moments M_{wheel} and the suspension forces F_{Susp}. In addition, it is necessary to consider the influence of the suspension on the camber angle, and predict the suspension forces by combining parameters such as suspension height and suspension height rate.

The final suspension forces act on the vehicle body. The combined action of suspension forces, gravity, wind resistance, and other external forces affects the position and attitude of the vehicle body.

In this process, it is necessary to consider the coordinate transformation of the suspension forces F_{Susp} when transmitted to the body model, the coupling effect of the center of mass, and the solution of the rotation matrix.

Based on the above data flow relationships, a complete 14-degree-of-freedom (14-DOF) dynamic model for the wheeled agricultural robot can be established. According to the model inputs, the ODE algorithm is used for numerical solution of the model, enabling accurate prediction of the overall position and attitude of the vehicle *(Xie et al., 2024)*.

Steering System Modeling

In this paper, the steering system is modeled based on the Ackermann geometric steering principle. As the primary input module of the overall system, the steering system plays a crucial role. The modeling of the Ackermann steering system not only involves the calculation of the wheel angle δ_s, but also provides the necessary data preparation for the subsequent tire model in terms of the sideslip angle α and slip ratio κ *(Aggarwal et al., 2020).* The specific calculation process is as follows:

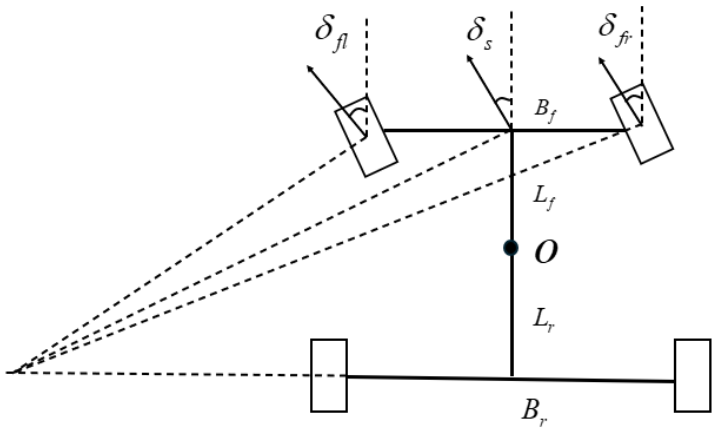

Fig. 2 -Schematic Diagram of the Ackermann Geometry Steering System

Formula for Calculating Wheel Angles:

$$\delta_{fl} = arctan\left\{\frac{2tan\delta_s(L_f + L_r)}{2(L_f + L_r) - B_f tan\delta_s}\right\} \quad (1)$$

$$\delta_{fr} = arctan\left\{\frac{2tan\delta_s(L_f + L_r)}{2(L_f + L_r) + B_f tan\delta_s}\right\} \quad (2)$$

where:

δ_s denotes the steering wheel angle, L_f and L_r represent the distances from the robot's center of gravity to the front axle and rear axle, respectively, and B_f is the front axle width. δ_{fl} and δ_{fr} represent the wheel angles of the left front wheel and right front wheel, respectively.

Based on the obtained wheel angles, the wheel sideslip angles can be solved.

$$\alpha_{fl} = -\left(\delta_{fl} - arctan\frac{v_{y\_fl}}{v_{x\_fl}}\right) \quad (3)$$

$$\alpha_{fr} = -\left(\delta_{fr} - arctan\frac{v_{y\_fr}}{v_{x\_fr}}\right) \quad (4)$$

$$\alpha_{rl} = arctan\frac{v_{y\_rl}}{v_{x\_rl}} \quad (5)$$

$$\alpha_{rr} = arctan\frac{v_{y\_rr}}{v_{x\_rr}} \quad (6)$$

where:

α_{fl} α_{fr} α_{rl} and α_{rr} represent the sideslip angles of the left front wheel, right front wheel, left rear wheel, and right rear wheel, respectively. v_{x_fl} v_{x_fr} v_{x_rl} v_{x_rr} represent the lateral velocities of the left front wheel, right front wheel, left rear wheel, and right rear wheel, respectively; v_{y_fl} v_{y_fr} v_{y_rl} v_{y_rr} denote the longitudinal velocities of the left front wheel, right front wheel, left rear wheel, and right rear wheel, respectively.

The velocity values in the sideslip angle formula are obtained from the following formulas:

Table 1

Formula for Wheel Center Velocity

Longitudinal Velocity of Wheel Center	Lateral Velocity of Wheel Center	Resultant Velocity
$v_{x\_fl} = v_x - \frac{B_f}{2}\omega_z$	$v_{y\_fl} = v_y + L_f\omega_z$	$v_{fl} = \sqrt{v_{x\_fl}^2 + v_{y\_fl}^2}$
$v_{x\_fr} = v_x + \frac{B_f}{2}\omega_z$	$v_{y\_fr} = v_y + L_f\omega_z$	$v_{fr} = \sqrt{v_{x\_fr}^2 + v_{y\_fr}^2}$
$v_{x\_rl} = v_x - \frac{B_r}{2}\omega_z$	$v_{y\_rl} = v_y - L_r\omega_z$	$v_{rl} = \sqrt{v_{x\_rl}^2 + v_{y\_rl}^2}$
$v_{x\_rr} = v_x + \frac{B_r}{2}\omega_z$	$v_{y\_rr} = v_y - L_r\omega_z$	$v_{rr} = \sqrt{v_{x\_rr}^2 + v_{y\_rr}^2}$

Formula for Solving Slip Ratio:

$$\kappa = \frac{\omega_{\omega\_ij}R_{\omega\_ij} - v_{\omega x\_ij}}{max\left(\omega_{\omega\_ij}R_{\omega}, v_{\omega x\_ij}\right)} \quad i = f,r \;\; j = l,r \tag{7}$$

where: ω_{ω_ij}denotes the tire angular velocity, R_ω is the effective tire radius, and $v_{\omega x\_ij}$ represents the tire lateral velocity.

Tire Model

Since the Magic Formula Tire Model is a semi-empirical formula based on experimental data, it not only exhibits high fitting accuracy within the range of conventional experiments but also remains applicable under certain extreme working conditions *(Cha et al., 2024)*. Therefore, this model is selected for tire modeling to predict the magnitude of forces acting on the robot body model, which is further used to derive the pose of the robot body. The Magic Tire Formula (Magic Formula) consists of nine components, Longitudinal Force (pure longitudinal slip), Lateral Force (pure side slip), Aligning Torque (pure side slip), Longitudinal Force (combined slip), Lateral Force (combined slip), Overturning Couple, Rolling Resistance Moment, Aligning Torque (combined slip), Vertical Load.

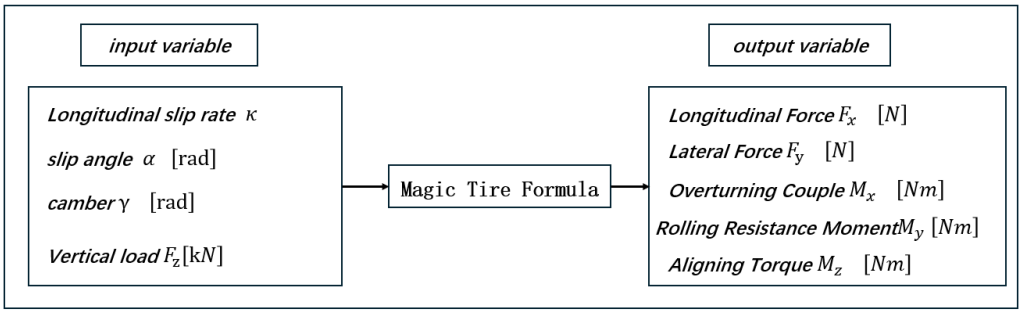

Fig. 3 - Relationship Between Input and Output Variables of the Magic Formula Tire Model

Based on the input-output relationship of the Magic Formula Tire Model illustrated in Fig. 3, the data conversion mechanism of the model can be briefly understood. The model involves the introduction of dimensionless parameters and intermediate derivation formulas, which are detailed in Eqs. (8–19). For the complete set of parameter definitions and detailed derivations of these formulas, refer to the third edition of the Pacejka Magic Formula, as reproducing all intermediate equations of this well-established tire model is unnecessary herein.

Under pure slip conditions, the relationship between the tire longitudinal force F_{xo}, longitudinal slip ratio κ, and tire vertical load F_z can be described as follows:

$$F_{xo} = D_x sin\left[C_x arctan\left\{B_x\kappa_x - E_x\left(B_x\kappa_x - arctan(B_x\kappa_x)\right)\right\}\right] + S_{Vx} \tag{8}$$

Under pure slip conditions, the relationship between the tire lateral force F_{yo}, tire sideslip angle α and tire vertical load F_z can be described as follows:

$$F_{yo} = D_y sin\left[C_y arctan\left\{B_y\alpha_y - E_y\left(B_y\alpha_y - arctan\left(B_y\alpha_y\right)\right)\right\}\right] + S_{Vy} \tag{9}$$

Under pure slip conditions, the relationship between the tire aligning torque M_{zo}, tire sideslip angle α and tire vertical load F_z can be described as follows:

$$M_{zo} = M'_{zo} + M_{zro} \tag{10}$$

M'_{zo} denotes the tire trail *(Roşca et al., 2022)*

$$M'_{zo} = -t_0 \cdot F_{yo} \tag{11}$$

M_{zro} denotes the residual torque:

$$M_{zro} = M_{zr}(\alpha_r) = D_r cos[C_r arctan(B_r \alpha_r)] \tag{12}$$

Under combined working conditions, the relationship between the tire longitudinal force F_x, longitudinal slip ratio α, and tire vertical load F_z can be described as follows:

$$F_x = G_{xa} \cdot F_{xo} \tag{13}$$

Under combined working conditions, the relationship between the tire lateral forceF_y, tire sideslip angle α, and tire vertical load F_z can be described as follows:

$$F_y = G_{yk} \cdot F_{yo} + S_{Vyk} \tag{14}$$

Overturning Couple:

$$M_x = F_z R_o \cdot \left(q_{sx1} - q_{sx2}\gamma^* + q_{sx3} F_y / F'_{zo}\right) \cdot \lambda_{Mx} \tag{15}$$

Rolling Resistance Moment;

$$M_y = F_z R_o \cdot \left(q_{sy1} arctan(v_r / v_o) + q_{sy2} F_y / F'_{zo}\right) \cdot \lambda_{My} \tag{16}$$

Under combined working conditions, the relationship between the tire Aligning Torque M_z, tire sideslip angle α, and tire vertical load F_z can be described as follows:

$$M_z = M'_z + M_{zr} + sF_x \tag{17}$$

M'_z denotes the tire trail:

$$M'_z = -t \cdot F'_y \tag{18}$$

M_{zr} denotes the residual torque:

$$M_{zr} = M_{zr}\left(\alpha_{r,eq}\right) = D_r cos\left[C_r arctan\left(B_r \alpha_{r,eq}\right)\right] \tag{19}$$

Furthermore, it has been found useful to introduce F_x and F_y interaction terms in the vertical stiffness *(Reimpell et al.,1986)*. For farmland scenarios involving deformable soil, the normal force calculation is optimized by integrating the Bekker formula *(Bekker, 1960)*—a classic model describing soil-bearing characteristics and tire-sinkage behavior. The revised formula for the normal force, incorporating horizontal force interaction, soil deformation effects, and overall stiffness functions, is proposed as follows:

$$F_N = |F_z| = \left\{1 + q_{V2}|\Omega|\frac{r_0}{V_0} - \left(q_{Fcx1}\frac{F_x}{F_{zo}}\right)^2 - \left(q_{Fcy1}\frac{F_y}{F_{zo}}\right)^2\right\}\left((q_{Fz1} + q_{Fz3}\gamma^2)\frac{\rho_z}{r_o} + q_{Fz2}\frac{\rho_z^2}{r_o^2}\right)F_{zo} \tag{20}$$

In Eq. (20) $\rho_z = max\left((r_0 - r_l + \Delta r)cos\gamma + r_c(1 - cos\gamma), 0\right)$, $\Delta r = q_{V1} r_0 (\Omega r_0 / V_o)^2$

Here, r_0 denotes the radius of the free non-rotating tire, r_l the loaded radius (distance between wheel centre and contact centre) and Δr the increase in free tyre radius due to wheel rotation velocity. The non-dimensional parameter q_{V1} governs the influence of tyre growth, q_{V2} the stiffness variation with speed, $q_{Fcx,y1}$ the interaction with horizontal forces and $q_{Fz1,2,3}$ the stiffness and non-linearity of the force deflection characteristic at zero speed and zero horizontal forces.

In Eq. (20) F_{zo} is derived from the Bekker formula model that describes the bearing characteristics and settlement laws of deformable soils (such as farmland and sandy land).

The specific formula is as follows:

$$F_{zo} = \frac{k_c}{b} + k_\phi \cdot z^{n-1} \tag{21}$$

Here, F_{zo} denotes the soil bearing pressure (kPa); k_c the cohesive modulus of soil (kN/m³); k_ϕ the frictional modulus of soil (kN/m⁴); b the width of contact area (m); z the soil sinkage (m); n the sinkage exponent (dimensionless), depending on soil type (e.g., (n≈0.5) for cohesive soil, (n≈1.0) for sandy soil).

Suspension Model

The interaction forces derived from tire force calculation need to be transmitted to the robot body model through the suspension system, and this process affects the response of the robot body part to the tire forces. In this paper, a linear suspension model *(Li et al., 2024)* is adopted. This model calculates the suspension force based on the relative height between the tires and the wheeled robot body, and the magnitude of the response force acting on the robot body part can be obtained through this model.

$$F_{WZ_{a,t}} = F_{zo_a} + k_{z_a}\left(z_{v_{a,t}} - z_{w_{a,t}} + m_{hsteer_a}\left|\delta_{steer_{a,t}}\right|\right) + c\left(\dot{z}_{v_{a,t}} - \dot{z}_{w_{a,t}}\right) \quad (22)$$

where F_{zo_a} is the vertical suspension spring preload, k_{z_a} is the spring constant, m_{hsteer_a} is the slope of the steering angle's influence on vertical force, $\delta_{steer_{a,t}}$ is the wheel steering angle, c is the vertical damping constant, $z_{v_{a,t}}$ and $\dot{z}_{v_{a,t}}$ are the vehicle relative displacement and velocity, respectively, and $z_{w_{a,t}}$ and $\dot{z}_{w_{a,t}}$ are the tire relative displacement and velocity, respectively.

It is assumed that the suspension is weightless, and the displacement and velocity of the suspension wheel are equal to the longitudinal velocity and lateral velocity of the vehicle, respectively. Thus, the following formula can be derived:

Table 2

Formulas for Force, Moment, Displacement-Velocity Relationships Between Tires and Wheeled Robot Body

Force	Moment	Displacement	Velocity
$F_{vx_{a,t}} = F_{wx_{a,t}}$	$M_{vx_{a,t}} = M_{wx_{a,t}} + F_{wy_{a,t}}\left(Re_{wy_{a,t}} + H_{a,t}\right)$	$x_{v_{a,t}} = x_{w_{a,t}}$	$\dot{x}_{v_{a,t}} = \dot{x}_{w_{a,t}}$
$F_{vy_{a,t}} = F_{wy_{a,t}}$	$M_{vy_{a,t}} = M_{wy_{a,t}} + F_{wy_{a,t}}\left(Re_{wy_{a,t}} + H_{a,t}\right)$	$y_{v_{a,t}} = y_{w_{a,t}}$	$\dot{y}_{v_{a,t}} = \dot{y}_{w_{a,t}}$
$F_{vz_{a,t}} = F_{wz_{a,t}}$	$M_{vz_{a,t}} = M_{wz_{a,t}}$		

where: Re is the effective tire radius, and H is the suspension height.

In addition, the suspension also affects the variation of the wheel camber angle, and their relationship is given by the following formula:

$$\gamma_{wz_{a,t}} = \gamma_{zo_a} + m_{hcamber_a}\left(z_{v_{a,t}} - z_{w_{a,t}} + m_{hsteer_a}\left|\delta_{steer_{a,t}}\right|\right) + m_{cambersteer_a}\left|\delta_{steer_{a,t}}\right| \quad (23)$$

where γ_{zo_a} is the initial camber angle, $m_{hcamber_a}$ is the slope of the relationship between the camber angle and the suspension height of front axle, m_{hsteer_a} is the slope of the relationship between the steering angle of axle a and the vertical force, and $m_{cambersteer_a}$ is the steering angle slope relative to front axle.

Robot Body Model

Since most agricultural robots are currently in the preliminary development stage, this study assumes the robot body model is a rigid body. Based on the forces and moments obtained from the steering system and tire model, these quantities are transmitted through the suspension system and then substituted into Eqs. (24–25) to solve for the state of the robot body model at each time step.

From the linear momentum theorem, the following expression can be obtained:

$$\vec{F}_b = \begin{bmatrix} F_x \\ F_y \\ F_z \end{bmatrix} = m\left(\dot{\vec{v}}_b + \vec{\omega} \times \vec{v}_b\right) = \begin{bmatrix} \dot{v}_x - v_y\omega_z + v_z\omega_y \\ \dot{v}_y - v_z\omega_x + v_x\omega_z \\ \dot{v}_z - v_x\omega_y + v_y\omega_z \end{bmatrix} \quad (24)$$

From the angular momentum (moment of momentum) theorem, the following relationship can be obtained:

$$\vec{M}_b = \begin{bmatrix} L \\ M \\ N \end{bmatrix} = I\dot{\vec{\omega}} + \vec{\omega} \times (I\vec{\omega})$$
$$= \begin{bmatrix} I_{xx}\dot{\vec{\omega}}_x - I_{xy}\dot{\vec{\omega}}_y - I_{xz}\dot{\vec{\omega}}_z - \omega_y\omega_z\left(I_{yy} - I_{zz}\right) - I_{yz}\left(\omega_y^2 - \omega_z^2\right) - \omega_x\left(I_{xz}\omega_y - I_{xy}\omega_z\right) \\ I_{yy}\dot{\vec{\omega}}_y - I_{xy}\dot{\vec{\omega}}_x - I_{yz}\dot{\vec{\omega}}_z - \omega_x\omega_z(I_{zz} - I_{xx}) - I_{xz}(\omega_z^2 - \omega_x^2) - \omega_y\left(I_{xy}\omega_z - I_{yz}\omega_x\right) \\ I_{zz}\dot{\vec{\omega}}_z - I_{yz}\dot{\vec{\omega}}_y - I_{xz}\dot{\vec{\omega}}_x - \omega_x\omega_y\left(I_{xx} - I_{yy}\right) - I_{xy}\left(\omega_x^2 - \omega_y^2\right) - \omega_z\left(I_{yz}\omega_x - I_{xz}\omega_y\right) \end{bmatrix} \quad (25)$$

In the right-hand side of the formula, the mass m and inertia tensor matrix I in Eqs. (24) and (25) need to be calculated separately.

The entire wheeled robot body is divided into 7 parts as shown in Fig. 4.

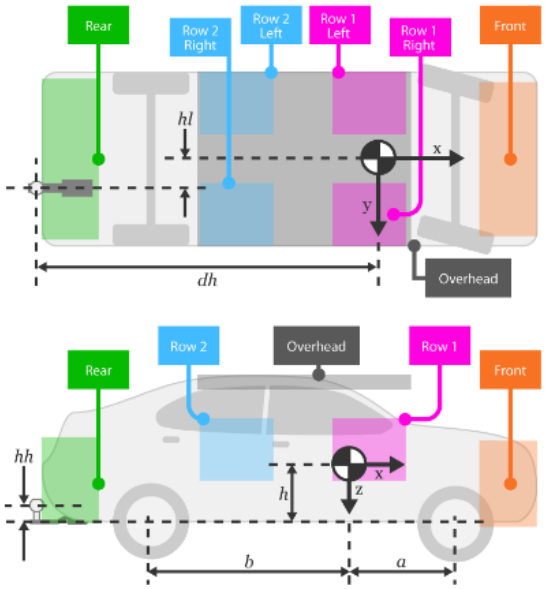

Fig. 4 - Schematic diagram of centroid mounting position and vehicle parameter dimensions of the wheeled robot

The centroid mass and centroid position of each part are measured respectively. The centroid position $\vec{R}$ is solved using the following formula:

$$\vec{R} = \begin{bmatrix} x \\ y \\ z \end{bmatrix} = \begin{bmatrix} \sum_{i=0}^{n} m_i x_i \\ \sum_{i=0}^{n} m_i y_i \\ \sum_{i=0}^{n} m_i z_i \end{bmatrix} \tag{26}$$

The calculation formula for the inertia tensor is:

$$I_i = \begin{bmatrix} I_{xx} & -I_{xy} & -I_{xz} \\ -I_{xy} & I_{yy} & -I_{yz} \\ -I_{xz} & -I_{yz} & I_{zz} \end{bmatrix} = \begin{bmatrix} \int\int (y_i^2 + z_i^2) d_y d_z & -\int\int (x_i y_i) d_x d_y & -\int\int (x_i z_i) d_x d_z \\ -\int\int (x_i y_i) d_x d_y & \int\int (y_i^2 + z_i^2) d_y d_z & -\int\int (y_i z_i) d_y d_z \\ -\int\int (x_i z_i) d_x d_z & -\int\int (y_i z_i) d_y d_z & \int\int (y_i^2 + z_i^2) d_y d_z \end{bmatrix} \tag{27}$$

The inertia tensor I is the sum of the inertia tensor of the centroid relative to the geometric center and the inertia tensor of the particle system relative to the centroid.

$$I = I_{center} + I_m \tag{28}$$

On the left-hand side of Eqs. (24–25), solving for the resultant external force $\vec{F}_b$ and resultant external moment $\vec{M}_b$ yields:

$$\vec{F}_b = \begin{bmatrix} F_x \\ F_y \\ F_z \end{bmatrix} = \begin{bmatrix} F_{dx} \\ F_{dy} \\ F_{dz} \end{bmatrix} + \begin{bmatrix} F_{gx} \\ F_{gy} \\ F_{gz} \end{bmatrix} + \begin{bmatrix} F_{extx} \\ F_{exty} \\ F_{extz} \end{bmatrix} + \begin{bmatrix} F_{FLx} \\ F_{FLy} \\ F_{FLz} \end{bmatrix} + \begin{bmatrix} F_{FRx} \\ F_{FRy} \\ F_{FRz} \end{bmatrix} + \begin{bmatrix} F_{RLx} \\ F_{RLy} \\ F_{RLz} \end{bmatrix} + \begin{bmatrix} F_{RRx} \\ F_{RRy} \\ F_{RRz} \end{bmatrix} \quad (29)$$

$$\vec{M}_b = \begin{bmatrix} M_x \\ M_y \\ M_z \end{bmatrix} = \begin{bmatrix} M_{dx} \\ M_{dy} \\ M_{dz} \end{bmatrix} + \begin{bmatrix} M_{gx} \\ M_{gy} \\ M_{gz} \end{bmatrix} + \begin{bmatrix} M_{extx} \\ M_{exty} \\ M_{extz} \end{bmatrix} + \begin{bmatrix} M_{FLx} \\ M_{FLy} \\ M_{FLz} \end{bmatrix} + \begin{bmatrix} M_{FRx} \\ M_{FRy} \\ M_{FRz} \end{bmatrix} + \begin{bmatrix} M_{RLx} \\ M_{RLy} \\ M_{RLz} \end{bmatrix} + \begin{bmatrix} M_{RRx} \\ M_{RRy} \\ M_{RRz} \end{bmatrix} + \vec{M}_F \quad (30)$$

In Eq. (28), the calculation formula for Gravity $\vec{F}_g$ is:

$$\vec{F}_g = \begin{bmatrix} F_{gx} \\ F_{gy} \\ F_{gz} \end{bmatrix} = DCM \cdot m \cdot \vec{g} \quad (31)$$

In Eq. (29), the calculation formula for Gravitational Moment $\vec{M}_g$ is:

$$\vec{M}_g = \begin{bmatrix} M_{gx} \\ M_{gy} \\ M_{gz} \end{bmatrix} = \vec{F}_g \times \vec{R} \quad (32)$$

$\vec{R}$ denotes the centroid position; DCM denotes the direction cosine matrix.

In Eq. (28), the calculation formula for Wind Force $\vec{F}_d$ is:

$$\vec{F}_d = \begin{bmatrix} F_{dx} \\ F_{dy} \\ F_{dz} \end{bmatrix} = \begin{bmatrix} -\frac{1}{2TR} C_d A_f P_{abs} (\overline{w})^2 \\ -\frac{1}{2TR} C_s A_f P_{abs} (\overline{w})^2 \\ -\frac{1}{2TR} C_l A_f P_{abs} (\overline{w})^2 \end{bmatrix} \quad (33)$$

In Eq. (29), the calculation formula for Wind Moment $\vec{M}_d$ is:

$$\vec{M}_d = \begin{bmatrix} M_{dx} \\ M_{dy} \\ M_{dz} \end{bmatrix} = \begin{bmatrix} -\frac{1}{2TR} C_{rm} A_f P_{abs} (\overline{w})^2 (a+b) \\ -\frac{1}{2TR} C_{pm} A_f P_{abs} (\overline{w})^2 (a+b) \\ -\frac{1}{2TR} C_{qm} A_f P_{abs} (\overline{w})^2 (a+b) \end{bmatrix} \quad (34)$$

In Eq. (32-33), the relative wind speed is used

$$\overline{w} = \sqrt{(\dot{x} - w_x)^2 + \left(\dot{y} - w_y\right)^2 + (w_z)^2} \quad (35)$$

where C_d, C_s, C_l are aerodynamic drag coefficients; C_{rm}, C_{pm}, C_{qm} are aerodynamic drag moment coefficients; A_f is the unit frontal thrust; P_{abs} is the ambient absolute pressure; T is the ambient air temperature; R is the atmospheric specific gas constant; and a, b are the distances from the robot's geometric center to the front and rear wheels, respectively.

The tire forces $\vec{F}_{FL}$, $\vec{F}_{FR}$, $\vec{F}_{RL}$, $\vec{F}_{RR}$ are derived from the Magic Tire Formula Eq. (8-21).

In Eq. (29), $\vec{M}_F$ is the moment derived from the Magic Tire Formula.

The tire moments $\vec{M}_{FL}$, $\vec{M}_{FR}$, $\vec{M}_{RL}$, $\vec{M}_{RR}$ are derived from $\vec{F}_{FL}$, $\vec{F}_{FR}$, $\vec{F}_{RL}$, $\vec{F}_{RR}$ and Eq. (20)

$$\vec{M}_i = \vec{F}_i \times \vec{R}_i \quad (36)$$

RESULTS

The modeling object selected in this study is the Ackermann front-steering drive-by-wire chassis Hunter SE developed by AgileX Robotics Co., Ltd., which has undergone secondary development to adapt to research needs. The AgileX wheeled robot has an overall mass of 100 kg, with a wheelbase of 890 mm and a track width of 350 mm; its chassis adopts a full electric drive configuration, powered by four in-wheel motors (one for each wheel), and is equipped with a 48 V 50 Ah lithium battery power supply system (with a maximum operating voltage of 54.6 V and a discharge cut-off voltage set at 43 V to avoid over-discharging). For on-board computing, the robot is fitted with a unit featuring an AMD Ryzen 7 4800H processor, 16 GB RAM, and

a single NVIDIA GeForce GTX 1650 Ti GPU—this setup supports real-time motion control, multi-sensor data processing, and algorithm operations such as autonomous navigation. The specific structure of the chassis is shown in the following figure.

Fig. 5 - Exterior of AgileX Robotics Mobile Chassis

Aiming at the problem that standard tire parameters can only characterize the dynamic characteristics of vehicles on hard road surfaces and are difficult to truly reproduce the dynamic responses under actual farmland conditions, it is necessary to construct a tire parameter model suitable for farmland scenarios through data collection and fitting under farmland conditions before simulation. Specifically, motion parameters such as tire rotational speed and wheel angle are collected by sensors, and mechanical sensors are arranged at the connection between the tire and the suspension to obtain wheel force data; based on the collected multi-dimensional data, the least squares method is adopted to complete the fitting of key tire parameters, and the unification of this parameter model with the tire model parameters in Carsim is realized simultaneously, which provides support for the accuracy of vehicle dynamics simulation under farmland conditions.

Double lane change (DLC) maneuver was selected, and a co-simulation comparison experiment using MATLAB and CarSim was conducted to verify the accuracy of the wheeled agricultural robot model. The figures below present the time-history curves of the steering wheel angle, yaw rate, vehicle body roll angle, and lateral acceleration, respectively.

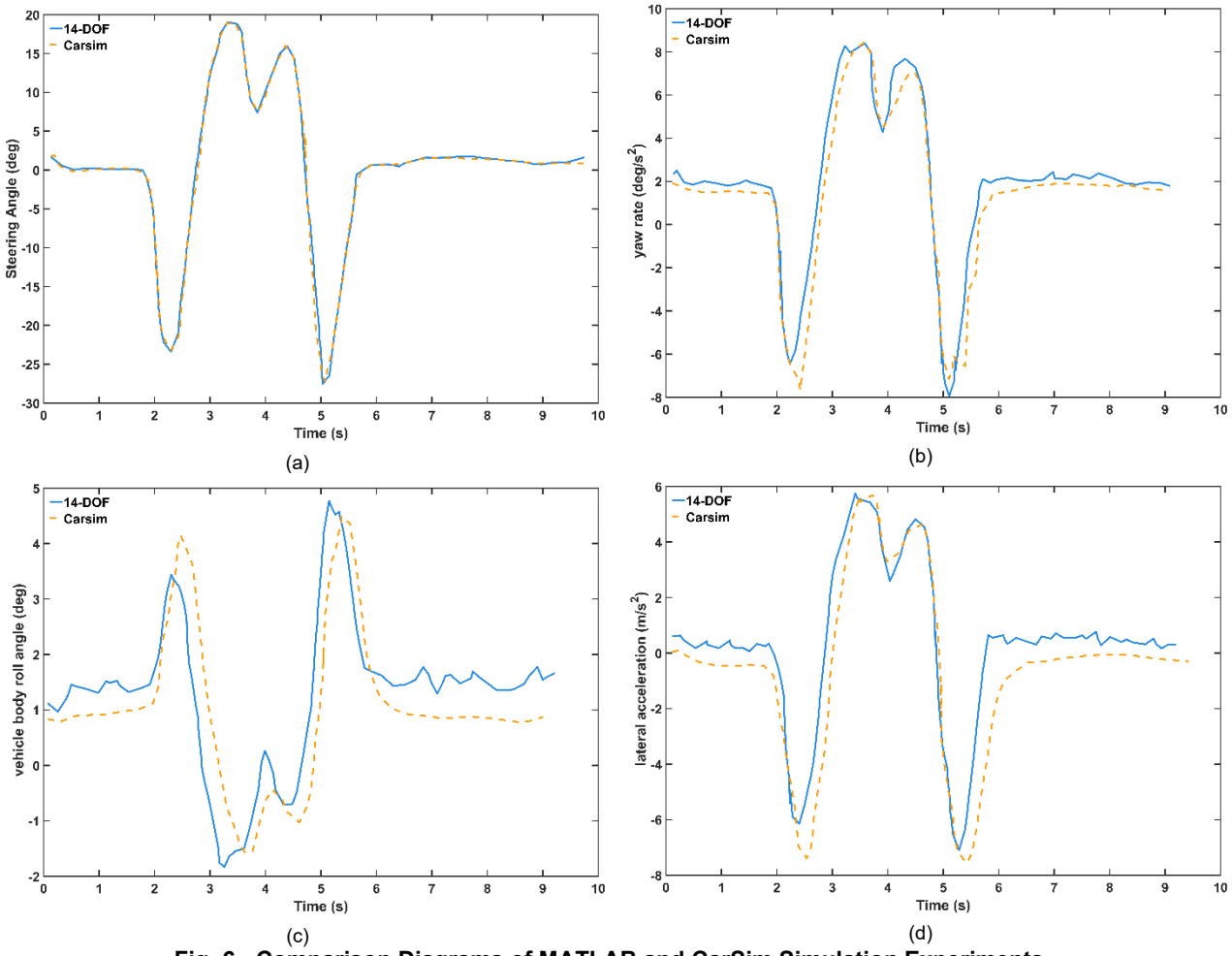

Fig. 6 - Comparison Diagrams of MATLAB and CarSim Simulation Experiments

(a) -steering wheel angle;(b) -yaw rate;(c) -vehicle body roll angle;(d) -lateral acceleration

Table 3

Error Table of Simulation Results Between MATLAB and CarSim

	Mean Absolute Error (MAE)
Steering wheel angle	$0.327°$
Yaw rate	$0.677°/s$
Vehicle body roll angle	$0.691°/s$
Lateral acceleration	$0.944\ m/s^2$

CONCLUSIONS

To address the limitation that simplified traditional agricultural robot models poorly adapt to complex farmland terrains and dynamic scenarios, this study proposes a 14-degree-of-freedom (14-DOF) wheeled robot model. By constructing four sub-modules (steering mechanism, tire, suspension, robot body) and establishing inter-module data flow, the model accurately predicts the robot's pose at any time, laying a theoretical foundation for optimal control.

Validation against CarSim (a widely recognized simulation tool) shows the mean error between the proposed model and CarSim is <1: steering wheel angle (0.327°), yaw rate (0.677°/s), lateral acceleration (0.944 m/s²), and body roll angle (0.691°). The maximum error is ≤1.5, with an error fluctuation range of ±0.3, meeting current simulation requirements.

Future work will derive an optimal control strategy based on this model to improve control robustness.

ACKNOWLEDGEMENT

The project supported by the R&D of low-speed unmanned autonomous navigation controller Project under Grant (No.2022TSGC1175).

REFERENCES

[1] Aggarwal, P., Sharma, P., & Siddhu, P. (2020). Ackermann steering system - A review. *International Journal of Trend in Scientific Research and Development,* 4(2), 240-241.

[2] Bekker, M. G. (1960). *Theory of land locomotion (Vol. 2).* University of Michigan Press.

[3] Bempah, S., Oduro, E., & Boateng, A. (2022). Dynamic modeling of a wheeled agricultural robot for precision farming. *Journal of Agricultural Engineering,* 53(2), 105-118.

[4] Cha, H., Kim, J., Yi, K. S., & Park, J. (2024). Investigation into high - performance tire characteristics at the limits of handling. *Vehicle System Dynamics,* 62(2), 428 – 447.

[5] Chen, W., Li, J., & Zhang, H. (2023). A 12-DOF dynamic model for agricultural robots considering soil-tire interaction. *Transactions of the Chinese Society of Agricultural Engineering,* 39(5), 123-131.

[6] Daum T. (2023). Mechanization and sustainable agri - food system transformation in the Global South. A review[J]. *Agronomy for Sustainable Development, 43(1): 16*.

[7] Ding, Y., & Wang, Z. (2021). Review of dynamic modeling techniques for agricultural mobile robots. *International Journal of Agricultural and Biological Engineering,* 14(3), 1-12.

[8] El-Ferik, S., & Shaheed, M. (2020*). Multi-body dynamics simulation of an agricultural robot using ADAMS. Engineering Science and Technology, an International Journal,* 23(4), 890-898.

[9] Hassaan, G. A., & Mohammed, N.A.A. (2015). Frequency Response of 10 Degrees of Freedom Full - Car Model for Ride Comfort. *International Journal of Scientific Research Engineering and Technology,* 4(1).

[10] Kayacan, E., Kayacan, E., Ramon, H., & Saeys, W. (2015). Towards agrobots: Identification of the yaw dynamics and trajectory tracking of an autonomous tractor. *Computers and Electronics in Agriculture,* 117, 155 - 165. doi:10.1016/j.compag.2015.07.011.

[11] Li, J., Dou, L., Zhao, Q., Qiao, B. (2024). Time Domain Analysis of Ride Comfort and Energy Dissipation Characteristics of Automotive Vibration Proportional–Integral–Derivative Control. *SAE International Journal of Vehicle Dynamics, Stability, and NVH,* 8(1), 49-61.

[12] Yi L., Razul S.G., Lin Z., See C.M.S. (2014). Target tracking in mixed LOS/NLOS environments based on individual measurement estimation and LOS detection,*" IEEE Trans. Wireless Commun.,* vol. 13, no. 1, pp. 99–111.

[13] Yi L., Razul S.G., Lin Z., See C.M.S. (2013). Individual a measurement detection algorithm for target tracking in mixed LOS/NLOS environments, *in Proc. IEEE Int. Conf. Acoust., Speech Signal Process. (ICASSP),* pp. 3924–3928.

[14] Yi L., Razul S.G., Lin Z., See C.M.S. (2013). Gating and robust EKF based target tracking in mixed LOS/NLOS environments, *in Proc. IEEE Int. Symp. Circuits Syst. (ISCAS),* pp.1364–1367.

[15] Yi L., Razul S.G., Lin Z., See C.M.S., (2012). Road-constraint assisted target tracking in mixed LOS/NLOS environments based on TDOA measurements, *in Proc. IEEE Int. Symp. Circuits Syst. (ISCAS*), pp. 2581–2584.

[16] L. Yi, Lim C.H., See C.M.S., Razul S.G., Lin Z., (2010). Robust tracking in mixed LOS/NLOS environments," *in Proc. IEEE Int. Conf. Robot. Autom. (ICARCV),* pp. 497–500.

[17] Long, Y. Z., Feng, J., Zhang, R.B., & Wei, T. (2022). Research on Torque Control of Four - wheel Driving EV based on Adaptive Disturbance Rejection Algorithm. *Mechanical Science and Technology for Aerospace Engineering,* 41(1), 75 - 81. doi:10.13433/j.cnki.1003 - 8728.20200625.

[18] Nigwal, D., Pasi, D. K., & Chouksey, M. (2023). Effect of nonlinear conical springs on the vibration characteristics of seven degree - of - freedom car model using MATLAB/Simscape. *Arabian Journal for Science and Engineering,* 48(3), 491 - 503. doi:10.1007/s40435-022-01007-2.

[19] Reimpell, J.S., Stoll, H., & Betzler, J.W. (2001). *The automotive chassis: engineering principles (2nd ed.). Oxford: Butterworth - Heinemann.*

[20] Roşca, R., Cârlescu, P., & Ţenu, I. (2022). The Improvement of a Traction Model for Agricultural Tire–Soil Interaction. *Agriculture,* 12(12), 2035. DOI: 10.3390/agriculture12122035.

[21] Sun, F., Meng, F., Ni, M., Zhao, Z., & Yi, L. (2025). Point cloud ground segmentation algorithm of vineyard agricultural robot based on surface fitting. *INMATEH - Agricultural Engineering,* 76(2). pp.69-78. https://doi.org/10.35633/inmateh-76-06.

[22] Xie, Z.L., Yin, W., & Wen, Z.W. (2024). ODE - based Learning to Optimize. *arXiv. https://arxiv.org/abs/2406.02006.*